How Does Aromaticity Rule the Thermodynamic Stability of Hydroporphyrins?

Nicolás Otero,[a] Stijn Fias,[b] Slavko Radenković,[b] Patrick Bultinck,[b] Ana M. Graña[a] and Marcos Mandado,*[a]

[a] *Department of Physical Chemistry, University of Vigo, Lagoas-Marcosende s/n, 36310 Vigo, Spain*

[b] *Department of Inorganic and Physical Chemistry, Ghent University, Krijgslaan 281 (S3), B-9000 Gent, Belgium*

Supporting information for this article is available on the WWW under http://dx.doi.org/10.1002/chem.2010xxxxx.

Keywords: porphyrins, aromaticity, electron delocalization, ring currents, resonance energy

Abstract

In this work several measures of aromaticity including energetic, magnetic and electron density criteria are employed to show how aromatic stabilization can explain the stability sequence of hydroporphyrins, ranging from porphin to octahydroporphin, and their preferred hydrogenation paths. The methods employed in this work are topological resonance energies and their circuit energy effects, bond resonance energies, multicenter delocalization indices, ring current maps, magnetic susceptibilities and nuclear independent chemical shifts. In order to compare the information obtained by the different methods the results have been put in the same scale by using recently proposed approaches. It has been found that all of them provide essentially the same information and lead to similar conclusions. Also, hydrogenation energies along different hydrogenation paths connecting porphin with octahydroporphin have been calculated using density functional theory. It is shown using the methods mentioned above that the relative stability of different hydroporphyrin isomers and the observed inaccessibility of octahydroporphin both synthetically and in nature can be perfectly rationalized in terms of aromaticity.

Introduction

Porphyrins are a unique class of compounds that are ubiquitous in nature and perform a wide variety of functions ranging from oxygen transport, electron transfer, and oxidation catalysts to photosynthesis.[1] They are among the most widely distributed and important cofactors found in nature and are crucial regulatory effectors in many biochemical processes. Hydroporphyrins are partly reduced derivatives of the porphyrin ring system in which one or more double bonds have been saturated by the formal addition of hydrogen atoms or alkyl groups across a double bond.[2] Several chemical differences between hydroporphyrins and porphyrins have been observed. For instance, hydroporphyrins have intrinsically larger core sizes and exhibit both a larger tendency to adopt nonplanar conformations and bigger displacements from planarity than the corresponding porphyrin complexes that have similar peripheral substitution.[3] Standard reduction potentials of ligand-centered redox processes generally decrease with increasing macrocycle saturation.[4] Thus, hydroporphyrin macrocycles are easier to oxidize and more difficult to reduce than porphyrins. The resistance of the macrocycle to reduction and the larger core size are reasons of why hydroporphyrins can stabilize metal ions in less common, low-valent oxidation states such as Cu(I) and Ni(I),[5] which are not readily accessible in porphyrins.

The most common naturally occurring hydroporphyrins are the dihydroporphyrins (chlorins) and the tetrahydroporphyrins (bacteriochlorins and isobacteriochlorins).[6] Depending on the hydrogenation sites one can distinguish different isomers of chlorin (**2a** and **2b** in Scheme 1) and bacteriochlorin (**3a** and **3c**). However, only one isomer of isobacteriochlorin (**3b**) is possible. Representative examples of these hydroporphyrins include chlorophyll, the ubiquitous chlorin that

regulates photosynthesis in green plants, algae, and cyanobacteria; bonellin, the sex-differentiating chlorin of the marine worm *Bonella viridis*;[7] bacteriochlorophyll and siroheme, the isobacteriochlorin prosthetic group of numerous sulfite and nitrite reductases.[8] Due to their favorable photophysical properties some members of the chlorin and bacteriochlorin families are also of medical interest. For instance, they have been shown to reverse tumor multidrug resistance and may find use in cancer chemotherapy.[9]

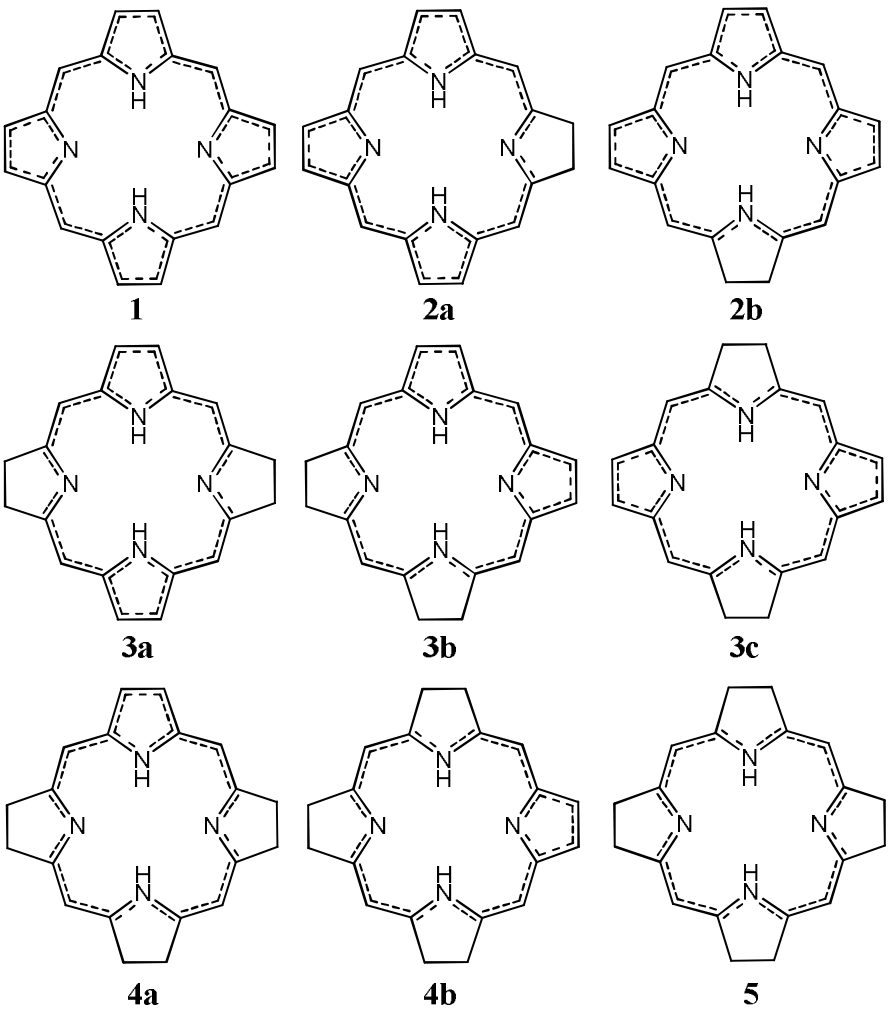

Scheme 1. Porphin (**1**) and the series of hydroporphirins (**2-5**)

On the other hand, in the wake of the investigation of the biosynthesis of vitamin B12 different forms of hexahydroporphyrins (derivatives of molecule **4a**) have also been synthesized.[10] The discovery, structural elucidation and chemistry of factor F 430, a dodecahydroporphyrin, has given an additional drive for the study of the chemistry of highly reduced porphyrins.[10] However, the missing links in the series of hydroporphinoid structures, octahydroporphin **5** and decahydroporphin has not been found yet.

There is no doubt that most of the physical and chemical properties of porphyrins and hydroporphyrins are intrinsically related to their aromatic character. Thus, two striking properties of the porphin ring (**1**), its visible electronic spectrum and NMR chemical shifts, are due to the delocalised π-electron system and its associated ring currents. Indirect evidence of currents in the porphin ring comes from experimental proton chemical shifts[11] and from calculations of the magnetic shielding at chosen points within the molecule.[12] Although the aromaticity of porphin has been extensively confirmed using different aromaticity criteria, the role played by all the possible aromatic pathways in the total aromaticity of porphin is still a controversial issue. Whereas the results obtained by some authors support the presence of a 18π-[16] annulene inner cross aromatic pathway with the C_2H_2 groups of the pyrrolic rings functioning only as exocylic bridges,[12a] other results support the existence of a bridged 18π-[18] annulene with the inner NH groups acting as inert bridges.[13]

A much smaller number of studies has been devoted to the study of the aromaticity in hydroporphyrins. Only a few addressed the topic in chlorin and bacteriochlorin using magnetic criteria[14,12b] and bond resonance energy, *BRE*.[15] Among previous studies on porphyrins it is worth mentioning the work by Aihara and co-workers using *BRE*s,[15] who quantified at the Hückel molecular orbital level the

relative weight of different aromatic pathways on the total aromaticity. Steiner, Fowler and co-workers have previously computed ring current maps for porphyrins, including bacteriochlorin[14] and ring current maps obtained in the present study will be compared to theirs. Although several works by these authors did explore several porphyrin derivatives,[16-18] they did not consider the complete hydrogenation series as discussed in the present study.

Hydrogenation of porphyrins mostly produces modifications of the electronic structure of the π system, which in turn changes the aromatic stabilization of the molecules. Then, it is expected that aromaticity plays a key role in the thermodynamic stability of hydroporphyrins. In this work we analyze in detail the aromatic character along the series of molecules represented in Scheme 1, paying special attention on the local aromaticity and their changes upon hydrogenation. Two main questions, essential for the understanding of the relative abundance of porphyrins in nature, are addressed in this paper; the relative stabilization of different isomers of hydroporphyrins **2**, **3** and **4** and the apparent thermodynamic instability of octahydroporphin **5**. Several methodologies comprising magnetic, energetic and electron density based aromaticity criteria are employed in this work, putting the different indices calculated in a common scale by using recently developed approaches[19] proposed independently or in common by some of the authors. The large set of methods employed here supports the reliability of the results obtained.

The paper is organized as follows: in the next section the methodologies employed are briefly reviewed; then the computational details are summarized; and in the third section the results obtained are presented and discussed. The main conclusions are formulated in the last section.

Methodology

Ring Current Maps

The existence of a ring current in a molecule is judged from the nature of the induced current density due to a magnetic field. As all molecules in the present paper have a closed shell singlet structure, one can limit the origin of the magnetic field to an external magnetic field. The induced electronic current density is then obtained as the expectation value of the operator[20]:

$$\hat{\mathbf{j}}(\mathbf{r}) = -\frac{1}{2}\sum_{i=1}^{N}\left[\hat{\boldsymbol{\pi}}_i \delta(\mathbf{r}_i - \mathbf{r}) + \delta(\mathbf{r}_i - \mathbf{r})\hat{\boldsymbol{\pi}}_i\right] \tag{1}$$

where the operator $\hat{\boldsymbol{\pi}}_i$ is given by:

$$\hat{\boldsymbol{\pi}}_i = \hat{\mathbf{p}}_i + \frac{1}{c}\mathbf{A}(\mathbf{r}_i) \tag{2}$$

and $\mathbf{A}(\mathbf{r}_i) = \frac{1}{2}\mathbf{B}\times(\mathbf{r}_i - \mathbf{d})$ is a vector potential that gives rise to the magnetic field. In the remainder we assume the Coulomb gauge is used. By virtue of the antisymmetry of the wave function, one obtains for the current density:

$$\mathbf{j}(\mathbf{r}) = -\frac{N}{2}\left\langle \Psi_0 \middle| \left[\hat{\boldsymbol{\pi}}_1 \delta(\mathbf{r}_1 - \mathbf{r}) + \delta(\mathbf{r}_1 - \mathbf{r})\hat{\boldsymbol{\pi}}_1\right] \middle| \Psi_0 \right\rangle \tag{3}$$

Under the assumptions already mentioned, the first order current density can be expressed as:

$$\begin{aligned}\mathbf{j}(\mathbf{r}) &= iN\int d\tau' \left[\Psi_0^{(0)}\nabla_1\Psi_0^{(1)} - \Psi_0^{(1)}\nabla_1\Psi_0^{(0)}\right] - \frac{1}{c}\mathbf{A}(\mathbf{r})\rho_0^{(0)}(\mathbf{r}) \\ &= \mathbf{j}^p(\mathbf{r}) + \mathbf{j}^d(\mathbf{r})\end{aligned} \tag{4}$$

where we used perturbation theory to the first order in the field, $\Psi_0 = \Psi_0^{(0)} + \Psi_0^{(1)}$, and integration goes over all electronic coordinates except the spatial coordinates of electron 1. The current density thus becomes a sum of a paramagnetic and a diamagnetic part. Keith and Bader[21a,21b] derived the current density in its first order for Hartree-Fock wave functions and subsequently introduced the so-called Continuous Set of Gauge Transformation (CSGT) method, later also described as the CTOCD-DZ or ipsocentric method[21], where the origin $\mathbf{d}$ for every point where the current density is evaluated is taken as itself, leading to the last term in (4) being zero. The reader is referred to the original work by Keith and Bader for details.[21a,21b] The total induced current density cannot change under such a transformation and Steiner et al.[22] have shown that the diamagnetic term is transferred to terms involving:

$$\int d\tau' \left(\Psi_0^{(0)} \nabla_1 \Psi_{0,d}^{(1)} - \Psi_{0,d}^{(1)} \nabla_1 \Psi_0^{(0)} \right) \tag{5}$$

For a single determinant wave function, one can interpret the induced current density in terms of orbital contributions where the paramagnetic contributions depend on the quantities[22]:

$$\left\{ \frac{\left\langle \psi_p^{(0)} \left| \hat{\mathbf{l}} \right| \psi_n^{(0)} \right\rangle}{\varepsilon_p - \varepsilon_n} \right\} \tag{6}$$

Where $\hat{\mathbf{l}}$ is the angular momentum operator, $\psi_p^{(0)}$ is a virtual orbital from the SCF procedure and the denominator is the energy difference between both orbital energies. The diamagnetic term depends on the set of terms:

$$\left\{ \frac{\left\langle \psi_p^{(0)} \left| \hat{\mathbf{p}} \right| \psi_n^{(0)} \right\rangle}{\varepsilon_p - \varepsilon_n} \right\} \tag{7}$$

Where $\hat{\mathbf{p}}$ is the usual linear momentum operator. This means that in the ipsocentric method, one can very easily interpret ring current data based on the availability of virtual orbitals of the right symmetry with respect to the symmetry of the direct product of the occupied orbital and the operator. Moreover, the orbitals involved need to be sufficiently close in energy to yield a small enough denominator in expression (6) or (7). Another appealing feature of the ipsocentric method is that only occupied-virtual orbital transitions are possible.[23] Obviously, the set of values in (6) and (7) do not wholly control the contribution of each orbital as there are also the terms as $\left\{\psi_{p/d}^{(0)}\nabla_1\psi_n^{(0)}\right\}$. The values (6) and (7) thus allow us to identify those orbitals that can contribute to the ring current based on symmetry arguments but not whether they will contribute significantly. We therefore report not only a transition diagram representing the different allowed transitions but also show orbital resolved ring current maps that also take in to account these terms.

Energy Effects of Cycles and Bond Resonance Energies

The extent of conjugation in a given circuit Z of a polycyclic conjugated π-electron system can be measured by the respective *energy effect* of the circuit, *ef*(*Z*).[24] The *ef*(*Z*)-quantity is defined as the difference between the total π-electron energy and an appropriate reference energy in which the contributions coming from the given circuit are neglected, whereas contributions coming from any other structural feature are taken into account. Using chemical-graph-theory tools within the Hückel molecular orbital (HMO) theory it can be shown that

$$ef(Z)=\frac{2}{\pi}\int_0^{\infty} ln\left|\frac{\phi(G,ix)}{\phi(G,ix)+2\phi(G-Z,ix)}\right|dx \qquad (8)$$

where *G* is the molecular graph representing the π-electron system considered, $\phi(G)$ is its characteristic polynomial and *G* - *Z* is the subgraph obtained by deleting from *G* the circuit *Z*. Details of the underlying theory, as well as an exhaustive bibliography can be found in the review[25] and in the recent papers.[26] On the other hand, the topological resonance energy, *TRE*,[27] is obtained by deleting from *G* all the possible circuits and measures the total aromatic stabilization of the system.

Bond resonance energy (*BRE*)[28] is another energetic quantity aimed at measuring the extent of π-electron conjugation in polycyclic systems. Within the HMO theory framework, *BRE* for a given π-bond between the atoms P and Q is calculated as the difference between the total π-electron energy and the energy of a hypothetical π-system constructed by setting $\beta_{PQ} = i\beta_{PQ}$ and $\beta_{QP} = -i\beta_{QP}$, where $\beta_{PQ} = \beta_{QP}$ is the resonance integral between the atoms P and Q. Calculated in this way, *BRE* represents a measure of stabilization or destabilization of the system considered due to π-electron conjugation along the circuits that share the given π-bond. The *BRE*-concept was elaborated and applied in numerous articles (see, for instance references [15,29]).

In the present work, the parameterization scheme for the heteroatoms proposed by Van-Catladge[30] is used, and calculated *ef*- and *BRE*-values are expressed in units of the HMO carbon-carbon resonance integral β_{CC}. Because β_{CC} is a negative quantity, positive *ef*- and *BRE*-values imply thermodynamic stabilization, whereas negative *ef*- and *BRE*-values imply thermodynamic destabilization of the given conjugated π-electron system.

Multicenter Delocalization Indices

Given an atomic partitioning of the molecular electron density, the multicenter delocalization indices,[31] *MCI*s, represent the extent to which the electrons are delocalized among a set of *n* atoms. Using the Mulliken partitioning scheme,[32] the *MCI* for a cycle of *n* atoms, Δ_n, adopts the following form,

$$\Delta_n = 2n\sum_{P}\left[\sum_{i\in A}\sum_{j\in B}\sum_{k\in C}\cdots\sum_{m\in M}(P^{\alpha}S)_{ij}(P^{\alpha}S)_{jk}\cdots(P^{\alpha}S)_{mi} + \right.$$

$$\left. + \sum_{i\in A}\sum_{j\in B}\sum_{k\in C}\cdots\sum_{m\in M}(P^{\beta}S)_{ij}(P^{\beta}S)_{jk}\cdots(P^{\beta}S)_{mi}\right] \qquad (9)$$

where $\mathbf{P}^{\alpha}$ and $\mathbf{P}^{\beta}$ are the so-called alpha and beta density matrices and **S** is the overlap matrix in terms of basis functions, *i*, *j*,... The first summation in Eq. (9) runs over all the non-equivalent permutations *P* of the *n* atoms. The remaining summations run over the basis functions centered on the atoms *A*, *B*, etc. Since the number of permutations increases rapidly with the number of atoms, the calculation of the multicenter index using Eq. (9) results unfeasible for large circuits. So, in these cases the use of the Giambiagi's ring index, I_n, [33]

$$I_n = \left[\sum_{i\in A}\sum_{j\in B}\sum_{k\in C}\cdots\sum_{m\in M}(P^{\alpha}S)_{ij}(P^{\alpha}S)_{jk}\cdots(P^{\alpha}S)_{mi} + \sum_{i\in A}\sum_{j\in B}\sum_{k\in C}\cdots\sum_{m\in M}(P^{\beta}S)_{ij}(P^{\beta}S)_{jk}\cdots(P^{\beta}S)_{mi}\right] \qquad (10)$$

where just the consecutive cyclic array of the atoms forming the ring is considered, is a good alternative for the determination of the multicenter electron delocalization.[19a,34] In addition, the value of the multicenter index shows a strong dependence on the number of centers and decreases dramatically as *n* increases.[31b] This makes multicenter indices difficult to compare with other aromaticity measures such as ring currents or *ef*(*Z*) or even among themselves if rings of different size are involved. The problem can be

partially solved using a recently proposed approach,[19a] where I_n is first normalized and then transformed to provide estimates of Aihara's circuit resonance energy, *CRE*,[35] given by,

$$CRE - MCI = \frac{1.332}{n} \frac{\left(I_n\right)^{n+1/n}}{\left(I_{n^0}\right)^{n+1/n^0}} \tag{11}$$

where I_{n^0} refers to Giambiagi's ring index of benzene (n^0 = 6), which is employed as reference.

In this paper we discuss the values of *CRE-MCI* as they contain the same chemical information as the *MCI* and can be compared directly to the *ef*(*Z*). The same approach was employed to estimate the ring current intensities, magnetic susceptibility exaltations (Eqs. (27) and (28) in reference [19a], respectively) and chemical shieldings from multicenter indices. The *zz*-component of the chemical shielding calculated at the center of a planar ring with n_b bonds can be approximated by the following expression,

$$\sigma_{zz}\left(\vec{r}_0\right) \approx A\left[\sum_{i=1}^{n_b} \frac{I_i}{\left|\vec{r}_i - \vec{r}_0\right|^2} sin\left(\theta_i\right)\right] \tag{12}$$

where I_i represents the current intensity (positive or negative for diatropic or paratropic sense, respectively) circulating through a given bond *i*, $\vec{r}_i$ is the position vector of the center of the bond and θ_i is the angle formed by the current vector at $\vec{r}_i$ and ($\vec{r}_i - \vec{r}_0$). *A* is a parameter that mainly depends on the magnetic field strength. Introducing the values of I_i obtained from multicenter indices in Eq. (12) one can estimate the value of the *zz* component of the nuclear independent chemical shift $NICS_{zz}$,[36] which is defined as $-\sigma_{zz}$. A similar idea was introduced previously by Fias et al. for the estimation of the

NICS at the center of a given ring from the *MCI* values of all the circuits encircling the ring.[19c]

Computational Details

Geometries and energies of the series of molecules **1**-**5** were obtained at the B3LYP/6-31++G(d,p) level using the Gaussian 03 program.[37] Energies and molecular symmetries can be seen in Table 1, whereas geometries have been incorporated in atomic Cartesian coordinates in the Supporting Information. As a remarkable feature we have found that hydrogenation of non-protonated pyrrol rings preserves the planar structure of the C-N skeleton of porphin, where hydrogenation of protonated pyrrol rings results in a distortion from planarity. However, the energy difference between planar and non-planar geometries is very small (between 0.1 and 0.5 kcal mol^{-1}). In the planar structures the molecular orbitals can be univocally classified as σ and π, so that ring currents and multicenter indices can be split up into σ and π contributions, the latter being related to the π-aromaticity of the system. For that reason we will only discuss the planar structures. $NICS_{zz}$ obtained at different points within the molecules and the *zz*-component of the magnetic susceptibility, χ_{zz}, were also calculated at the B3LYP/6-31++G(d,p) level.

Calculations of ring currents and multicenter indices were performed using a minimal basis set (STO-3G) and own Fortran routines requiring as only input formatted checkpoint files from Gaussian 03. The required two-electron integrals for the ring currents are obtained from locally modified codes from the BRABO ab initio package.[38] The reason for such reduction of the basis set size in these calculations is

merely computational. It has been proven for the calculation of ring currents[19,39] and multicenter indices[19,40] that a minimal basis set provides essentially the same information as other larger basis sets with a much lower computational effort. This is because the main important factors here are the symmetry and the shape of the molecular orbitals. Symmetry does not depend on the basis set and the shape of the orbitals is not significantly altered by the number of basis functions employed. Even using the pseudo-π method[39,40], where carbons are replaced by hydrogens and the STO-3G basis set is employed, one captures the same essential information about the ring currents and multicenter electron delocalization in polycyclic aromatic hydrocarbons. Unfortunately, the pseudo-π method is not applicable to porphyrins because we have to distinguish between nitrogen and carbon atoms. We always consider a magnetic field in the *z*-direction (perpendicular to the plane formed by the C-N skeleton) and compute the perturbed orbitals using the first order coupled Hartree-Fock approach (FO-CHF). Ring currents are plotted on a grid in the *xy* plane with a diatropic current represented by a counterclockwise circulation.

Multicenter indices and energy effects of cycles were calculated for all the circuits represented in Figure 1. Then, *CRE-MCI* values were obtained using Eq. (11), current intensities and magnetic susceptibilities were estimated from the *MCI* values following the procedure described in reference [19a] and $NICS_{zz}$ values were estimated from Eq. (12). Ring current maps as well as *MCI*s were both separated into σ and π contributions, and the results obtained for the latter are presented in the next section. Orbital resolved ring current maps were also calculated for all molecules.

Results and Discussion

Taking into account that the isomerisation of the hydroporphyrins of Scheme 1 does not entail a significant change of entropy, we will employ the molecular electronic energy to establish the relative thermodynamic stability of different isomers. Thus, the molecular electronic energies collected in Table 1 clearly reflect that the most stable isomers correspond to the molecules labelled by "**a**". It means that the hydrogenation of non-protonated pyrrol rings is thermodynamically favoured over the hydrogenation of protonated pyrrol rings throughout the series. Although not a new finding but a confirmation of experimental observations, elucidating whether aromaticity is responsible for the relative stability is one of the main goals of this work. A first proof of the important role played by the aromatic stabilization in hydroporphyrins can be found in the values of the *TRE* collected in Table 1. They reflect the same stability sequence as the *ab initio* energies, even the *TRE* is able to predict the small destabilization of the isomer **3b** with respect to **3a** and a much larger destabilization of the isomer **3c**.

There are many ways of accounting for the relative aromatic stabilization of isomers. However, the difference between the isomers considered in this work is just the hydrogenation site, and then the most suitable quantity seems to be the *BRE* of the C-C bond involved in the process. Thus, all the hydrogenation paths linking the hydroporphyrins of Scheme 1 are summarized in Figure 2 and confronted with the *BRE*s and the *ab initio* hydrogenation energies involved. The hydrogenation energies were calculated as the difference between the electronic energy of the hydrogenated product and the summation of the electronic energy of the non-hydrogenated reactant plus the electronic energy of the isolated hydrogen molecule. As mentioned in the "Computational Details" section only the planar structures were employed in the

calculations. In the figure the thermodynamically favoured paths are denoted by solid arrows whereas the unfavoured ones are denoted by dashed arrows. In all cases the favoured hydrogenation coincides with the smallest *BRE* value, which means that the hydrogenation occurs on the C-C bond where the entailing aromatic destabilization is smaller. Figure 2 shows that the most stable products resulting from the progressive hydrogenation of porphin correspond to the series **2a**-**3a**-**4a**. The hydrogenation of **4a** to give **5** is energetically unfavoured with a positive hydrogenation energy and a quite large value of the *BRE*. Moreover, the entropic contribution to the Gibbs free energy is expected to disfavour even more the hydrogenation process, at least within the ideal gas phase model. On the contrary, the hydrogenation of **4b** to give **5** is energetically feasible, but the previous formation of **4b** is unlikely according to the energies presented in Figure 2.

The *BRE* of a given bond can be analyzed in detail with the energy effects of the circuits that share the bond. All the possible circuits are represented in Figure 1 for the porphin molecule, but depending on the hydrogenation sites some of them may not appear in the corresponding hydroporphyrin. The *ef*(*Z*) and *CRE-MCI* values calculated for these circuits are collected in Table 2. First, we must mention that there are important discrepancies between both quantities. Thus, according to the *ef*(*Z*) values the aromatic stabilization of protonated pyrrol rings is larger than that of non-protonated pyrrol rings except for molecules **2a** and **3b**. On the contrary, the *CRE-MCI* values do not reflect important differences between both, being in general larger for the protonated pyrrol. The *ef*(*Z*) values associated to the macrocycles are in general larger than the *CRE-MCI* values, with the exception of porphin and the naturally occurring hydroporphyrins (chlorin (**2a)** and bacteriochlorin (**3a**)) where the values are quite

similar. In spite of these differences, a similar explanation for the relative stabilization of the isomers is extracted from the *ef*(Z) and *CRE-MCI* values. Thus, in both cases the aromatic stabilization of macrocycles **IV** (17 centers), **VI** (18 centers) and **IX** (19 centers) is significantly larger than that of the corresponding macrocycles **V** (17 centers), **VII** and **VIII** (18 centers) and **X** (19 centers) for all the isomeric series. Macrocycles **IV**, **VI** and **IX** encircle the protonated pyrrol rings and leave out the non-protonated ones, contributing to the resonance energy of the C_β-C_β bonds in the former. On the contrary, macrocycles **V**, **VII** and **X** encircle the non-protonated pyrrol rings and leave out the protonated ones, contributing to the resonance energy of the C_β-C_β bonds in the former. The result is that hydrogenation of protonated pyrrol rings breaks the cyclic electron delocalization in macrocycles with stronger π-electron conjugation, which entails a larger aromatic destabilization. This is in fact in agreement with qualitative information obtained from traditional non-polar Kekulé structures in combination with the conjugated circuits model.[41] According to the conjugated circuits model, only rings supporting conjugated circuits are expected to contribute significantly to the aromatic stabilization. In our case, it is not possible to identify conjugated circuits encircling the rings **V**, **VII**, **VIII** and **X**, and then these rings are expected to provide a smaller aromatic stabilization. In recent contributions some of the authors showed the connection existing between conjugated circuits and measures of aromaticity such as *MCI*s[42] and ring currents[43] in polycyclic aromatic hydrocarbons.

The most remarkable difference between *ef*(*Z*) and *CRE-MCI* values is found in the macrocycle **III**, the central 16-center ring, in molecule **5**. The *CRE-MCI* predicts a much lower aromatic stabilization associated to this macrocycle than the *ef*(*Z*). This seems to reflect a divorce between aromatic stabilization and electron delocalization. In

principle the absence of conjugated circuits in this macrocycle should be reflected by a relatively small electron delocalization. This is true for molecules **1**, **2a**, **2b**, **3a**, **3b** and **4a**, where the *ef*(*Z*) and *CRE-MCI* values of cycle **III** are lower than those of cycles **IV** and **VI**. The fact that these cycles contain a larger number of centers than cycle **III**, so decreasing their relative aromatic stabilization, reinforces the result. However, the *ef*(*Z*) of molecule **5** is remarkably large and does not come with a parallel increase of the π-electron delocalization. The aromatic stabilization due to the π-conjugation in this circuit is significantly large but the electron delocalization is still small in agreement with the qualitative predictions. It must be mentioned here that results obtained by Jusélius et al. using the aromatic ring current shielding (ARCS) method[12b] also pointed out to that an aromatic pathway corresponding to cycle **III** (a 18π-[16]annulene inner cross) only exists in the octahydroporphin **5**.

Measures of the magnetic response of the system can shed light on the contradictions between aromatic stabilization and electron delocalization in these systems. *Ab initio* π-ring currents are represented in Figure 3 and the translational and rotational transitions based on expressions (6) and (7), respectively, are depicted in Figure 4. The π-ring current map of porphin (**1)** shows a ring current that is bifurcated around the protonated pyrrol rings, the current being somewhat stronger at the outer side of the ring. In the non-protonated pyrrol rings, however, the current remains at the inside of the ring, with virtually no π-current running through the outer side of the ring. The ring current mainly originates from the translational transitions from the HOMO and HOMO-1 to the LUMO and LUMO+1 (see Figure 4). Apart from these, there is a relatively small rotational transition from the HOMO-2 to the LUMO, corresponding to a paratropic current encircling the two non-protonated pyrrol rings. The observed

bifurcation is in agreement with the findings by Steiner and Fowler.[14] Their interpretation of the ring current in terms of only four active electrons is also in good agreement with the diagram presented in figure 4. Steiner and Fowler did not mention the small rotational transition although our diagram also shows that this contribution is likely very small due to the larger energy difference between the two molecular orbitals involved. Figure 5 indeed also confirms that the HOMO-2 contribution to the ring current is very small.

When hydrogenating a non-protonated pyrrol ring of porphin (to form dihydroporphin **2a**), the π-ring current pattern remains unchanged. Examining the diamagnetic and paramagnetic contributions shows that the HOMO-2 to the LUMO rotational transition has disappeared. Instead, two small rotational transitions from the HOMO and HOMO-1 are present (HOMO to LUMO and HOMO-1 to LUMO+1). This blocking of a pathway in **2a** compared to **1** is in agreement with previous work by Steiner and Fowler.[14a] Hydrogenating a protonated pyrrol ring on the other hand largely annihilates the ring current of the molecule **2b**. Besides becoming smaller, the bifurcation around the non-protonated pyrrol ring is lost, the ring current running over the outer side of the ring. The HOMO-LUMO gaps of molecules **2a** and **2b** are more or less the same and thus do not explain the change in the ring current. The reason for the dramatic change can be seen in the transition-diagram, which shows how the translational transitions become smaller compared to molecule **2a** and how the HOMO to LUMO rotational transition becomes stronger. Moreover, there is the same small rotational transition from the HOMO-2 to the LUMO as in porphin, diatropically encircling the two non-protonated pyrrol rings.

Hydrogenating the second non-protonated pyrrol ring of **2a** (to form tetrahydroporphin **3a**), once again has no impact on the form of the π-ring current

pattern. The HOMO-LUMO gap is smaller than that of molecule **2a**, the translational transitions are larger (possibly due to the smaller HOMO-LUMO gap) and the rotational transitions are gone. This explains the somewhat larger ring current compared to molecule **2a**.

Tetrahydroporphin **3b**, like dihydroporphin **2b**, has smaller translational transitions and a large HOMO to LUMO rotational transition, explaining the small ring current of the molecule. The HOMO-2 to the LUMO rotational transition is no longer present, but a small HOMO-1 to LUMO+1 rotational transition can be seen. Molecule **3b** also has the largest HOMO-LUMO gap of the molecules **3a-c**.

Tetrahydroporphin **3c** has a strong diamagnetic ring current pattern, following macrocycle **III**. The molecule has a much smaller HOMO-LUMO gap than molecules **3a** and **3b**. It has strong translational transitions from the HOMO and HOMO-1 to the LUMO and LUMO+1 (possibly due to the smaller HOMO-LUMO gap) and the same small rotational transition from the HOMO-2 to the LUMO as in porphin and molecule **2b**, encircling the two non-protonated pyrrol rings.

Hexahydroporphins **4a** and **4b** both have a relatively weak ring current, the one of **4b** being somewhat larger than that of **4a**. Both molecules have small translational transitions compared to the other molecules and both have two rotational transitions from HOMO to LUMO+1 and from HOMO-1 to LUMO. Molecule **4b** has the smallest HOMO-LUMO gap and two important extra HOMO-2 to LUMO and LUMO+1 translational transitions, explaining the larger ring current.

Octahydroporphin **5**, like tetrahydroporphin **3c**, has a strong diamagnetic ring current pattern, following macrocycle **III**. The molecule only has large translational transitions from the HOMO and HOMO-1 to the LUMO and LUMO+1.

The *ab initio* ring current plots can be compared with the pictorial representation of the ring currents obtained from multicenter indices (represented in Figure 5). In this figure the arrows represent both the sense and the relative strength of the current intensity circulating through each bond. The intensity for a given bond is obtained by summation of the I_i values, estimated using multicenter indices, of all circuits containing the bond.

As one can see comparing Figure 3 and Figure 5, there is a good correspondence between *MCI*s and ring currents for most of molecules. However, multicenter indices predict a remarkably smaller current intensity in octahydroporphin **5**, similar to that of hexahydroporphin **4a**. As one can see in the figure, the same happens for tetrahydroporphin **3b**. An explanation for this disagreement can be found in the analysis of the orbital interactions. There are two necessary conditions for a strong ring current; large values for some of the integrals between occupied and virtual orbitals presented in expressions (6) and (7), and a small energy gap between these orbitals. The second condition causes the ring current to be mainly produced by interactions between the highest occupied orbitals and the lowest virtual orbitals. The MCI depends only on the first order density matrix, which does not contain explicitly information on the virtual orbitals. Hence, the MCI and derived quantities cannot reflect all subtleties that differentiate among molecules.

We have depicted in Figure 6 the orbital contributions to the ring current from the four highest energy occupied orbitals of molecules **1**, **4a** and **5** (the complete orbital resolved ring currents for all molecules can be found in the Supporting Information). As one can see, only two orbitals (HOMO and HOMO-1) have a significant contribution to the ring current. These orbitals yield a strong current density along the central ring for molecules **1** and **5**, whereas the current density is significantly smaller for molecule **4a**.

We are now in position to state that, even when two hydroporphyrins present similar ring electron delocalization, they can display significantly different ring current densities if their occupied-virtual orbital interactions differ substantially.

On the other hand, we have replaced the values of the *CRE-MCI* by the *ef*(*Z*) to represent the current intensity in molecules **4a** and **5** and to check if discrepancies also appear using energy effects. This is not however completely supported by theory as the mathematical relation between electron current intensity and energy stabilization due to cyclic electron conjugation was established by Aihara[35] using the circuit resonance energy, *CRE*, which differs from the Gutman's definition of *ef*(*Z*). However, both quantities usually correlate and are expected to provide very similar information. As one can see in Figure 5, the *ef*(*Z*) values predict the stronger current in molecule **5**. There is however a discrepancy with the ring current maps that is corrected using multicenter indices. Thus, the paratropic sense of the current circulating by the C-N(H)-C unit in the non-hydrogenated pyrrol ring of **4a** is wrongly represented using the *ef*(*Z*) values but correctly represented with multicenter indices.

Additional proof of the differences in the magnetic response of molecules **4a** and **5** can be obtained from the values presented in Table 3 for the magnetic susceptibility and $NICS_{zz}(1)$ calculated one angstrom over the center of the molecule. The center of the molecule was chosen as the position of the ring critical point of the electron density corresponding to the central ring.

The *zz* component of the magnetic susceptibility tensor is slightly larger for **5** than for **4a**, even though the large differences in the ring currents are not reflected on the magnetic susceptibilities. On the other hand, the $NICS_{zz}(1)$ calculated at the central ring is significantly larger for **5** than for **4a**. However, both the magnetic susceptibility

and the $NICS_{zz}(1)$ are significantly smaller for molecule **5** than for molecules **1**, **2a** and **3a**, differences that do not match well the ring current plots. It must be also mentioned that the $NICS_{zz}(1)$ values calculated at the center of the non-hydrogenated pyrrol rings increases when going from **1** to **5** (see values in Table 3), which is in agreement with the parallel increase of the *CRE-MCI* and *ef*(*Z*) values for these rings.

Going back to Figure 3, one can glimpse that differences between magnetic and electron density criteria of aromaticity for the series of hydroporphyrins only affect molecules **5** and **3c.** Comparing magnitudes such as magnetic susceptibilities and *NICS* can help to confirm this observation. Thus, the magnetic susceptibility exaltations obtained from multicenter indices, $\chi_{\text{-MCI}}$, correlate perfectly with the *ab initio zz* component of the magnetic susceptibility tensor. It can be seen in Figure 7 that only molecules **3c** and **5** display a noticeable deviation. In spite of the worse regression coefficient, the correlation found between *ab initio* $NICS_{zz}(1)$ and *NICS* estimated from multicenter indices is even more remarkable. Taken into account the rough approximations introduced in Eq. (12) for the calculation of the magnetic shielding, the correlation shown in Figure 7 can be considered quite satisfactory. Once again, molecules **3c** and **5** are the ones displaying important deviations.

It must be mentioned that we have also replaced the *CRE-MCI* values by the *ef*(*Z*) to get similar representations to those of Figure 7. The correlations obtained using *ef*(*Z*) were significantly worse than those obtained with *CRE-MCI*, which indicates that even though the circuit energy effects account for the different magnetic response of molecules **4a** and **5**, multicenter indices correlate in general better with magnetic indices. The fact that energy effects lead to a worse representation of the magnetic response of the systems investigated here could be related to the level of calculation. In

porphyrins and hydroporphyrins the presence of heteroatoms and hydrogenated rings is difficult to account for with the limitations of the HMO level.

Conclusions

The relative stability of different hydroporphyrin isomers as well as the naturally and synthetically inaccessibility of octahydroporphin (**5**) have been explained in terms of total and local aromaticity by using a large variety of methods, including energetic, magnetic and electron density criteria.

By partitioning the total aromaticity into individual circuit contributions it was concluded that aromaticity alone can explain why the hydrogenation of non-protonated pyrrol rings is always favoured over that of protonated pyrrol rings in porphyrins and hydroporphyrins. Although the local contribution to the aromaticity of pyrrol cycles is significantly larger than that of the macrocycles that connect the pyrrol units, the latter play a crucial role in the relative stability of the different isomers.

The hydrogenation energies along the different hydrogenation paths connecting porphin with octahydroporphin (**5**) have been analyzed. The conclusion is that formation of (**5**) is energetically unfavoured, and that the energy destabilization associated to the disruption of the electron conjugation upon hydrogenation can perfectly explain this fact.

Analysis of the electron delocalization and different magnetic response properties lead to the same conclusions as the measures of aromatic stabilization energy. In order to compare the different methods we have put their information in the same scale by using some recently proposed approaches. Only for molecules (**3c**) and (**5**) the

different methods employed differ substantially, even though this fact does not affect the general conclusions obtained.

Acknowledgments

Free access to computational resources of Centro de Supercomputación de Galicia (CESGA) and services at Ghent University (Stevin Supercomputer Infrastructure) are gratefully acknowledged. PB thanks the FWO Vlaanderen for continuous support to his group and the help of C. Van Alsenoy for local implementation of the 2-electron integrals. AG and MM thanks the Xunta de Galicia and University of Vigo for financial support to their group. MM thanks the "Xunta de Galicia" for his contract as researcher in the "Isidro Parga Pondal" program. NO thanks the University of Vigo for a predoctoral fellowship. Special thank to Prof. Ricardo Mosquera for helpful discussions during the elaboration of this work.

References

[1] *The Porphyrin Handbook* (Eds: K. M. Kadish, K. M. Smith, R. Guilard), Academic Press: San Diego, 2000, **2004**.

[2] H. Scheer, *The Porphyrins* (Ed: D. Dolphin), Academic Press: New York, **1978**, Vol. 2, pp 1-44.

[3] a) W. R. Scheidt, Y. J. Lee, *Struct. Bonding (Berlin)* **1987**, *64*, 1. b) A. M. Stolzenberg, L. J. Schussel, J. S. Summers, B. M. Foxman, J. L. Petersen, *Inorg. Chem.* **1992**, *31*, 1678. c) A. M. Stolzenberg, G. S. Haymond, *Inorg. Chem.* **2002,** *41*, 300.

[4] a) P. F. Richardson, C. K. Chang, L. D. Spaulding, J. Fajer, *J. Am. Chem. Soc.* **1979**, *101*, 7736. b) A. M. Stolzenberg, L. O. Spreer, R. H. Holm, *J. Am. Chem. Soc.* **1980**, *102*, 364. c) C. K. Chang, J. Fajer, *J. Am. Chem. Soc.* **1980**, *102*, 848. d) A. M. Stolzenberg, S. H. Strauss, R. H. Holm, *J. Am. Chem. Soc.* **1981**, *103*, 4763. e) C. K. Chang, L. K. Hanson, P. F. Richardson, R. Young, J. Fajer, *Proc. Natl. Acad. Sci. U.S.A.* **1981**, *78*, 2652.

[5] a) A. M. Stolzenberg, M. T. Stershic, *Inorg. Chem.* **1987**, *26*, 3082. b) A. M. Stolzenberg, M. T. Stershic, *J. Am. Chem. Soc.* **1988**, *110*, 6391. c) A. M. Stolzenberg, L. J. Schussel, *Inorg. Chem.* **1991**, *30*, 3205.

[6] a) A. R. Battersby, *Nat. Prod. Rep.* **2000**, *17*, 507. b) F.-P. Montforts, B. Gerlach, F. Höper, *Chem. Rev.* **1994**, *94*, 327.

[7] L. Agius, J. A. Ballantine, V. Ferrito, V. Jaccarini, P. Murray-Rust, A. Pelter, A. F. Psaila, P. J. Schembri, *Pure Appl. Chem.* **1979**, *51*, 1847.

[8] a) M. J. Murphy, L. M. Siegel, *J. Biol. Chem.* **1973**, *248*, 6911. b) M. J. Murphy, L. M. Siegel, S. R. Tove, H. Kamin, *Proc. Natl. Acad. Sci. U.S.A.* **1974**, *71*, 612.

[9] M. R. Prinsep, F. R. Caplan, R. E. Moore, G. M. L. Patterson, C. D. Smith, *J. Am. Chem. Soc.* **1992**, *114*, 385.

[10] See reference [6b] and references therein.

[11] H. Scheer, J. J. Katz, *Nuclear Magnetic Resonance Spectroscopy of Porphyrins and Metalloporphyrins*: in *Porphyrins and Metalloporphyrins* (Ed.: K. E. Smith), Elsevier, Amsterdam, **1975**, pp 399.

[12] a) M. K. Cyrañski, M. Krygowski, M. Wisiorowski, N. J. R. van Eikema Hommes, P. von R. Schleyer, *Angew. Chem. Int. Ed.* **1998**, *37*, 177. b) J. Jusélius, D. Sundholm, *Phys. Chem. Chem. Phys.* **2000**, *2*, 2145.

[13] a) E. Vogel, W. Haas, B. Knipp, J. Lex, H. Schmickler, *Angew. Chem. Int. Ed. Engl.*, **1988**, *27*, 406. b) E. Vogel, *J. Heterocycl. Chem.*, **1996**, *33*, 1461. c) T. D. Lash, S. T. Chaney, *Chem. Eur. J.*, **1996**, *2*, 944. d) T. D. Lash, J. L. Romanic, J. Hayes, J. D. Spence, *Chem. Commun.*, **1999**, 819.

[14] a) E. Steiner, P. W. Fowler, *Mapping the Global Ring Currents in Porphyrins and Chlorins:* in *Chlorophylls and Bacteriochlorophylls: Biochemistry, Biophysics, Functions and Applications (Advances in Photosynthesis and Respiration)* (Eds: B. Grimm, R. J. Porra, W. Rüdiger, H. Scheer), Springer, Dordrecht, **2005**, Vol 25, pp. 337–347. b) E. Steiner, P. W. Fowler, *ChemPhysChem*, **2002**, *3*,114.

[15] J. Aihara, M. Makino, *Org. Bio. Chem.*, **2010**, *8*, 261.

[16] E. Steiner, A. Soncini, P. W. Fowler, *Org. Biomol. Chem.*, **2005**, *3*, 4053.

[17] E. Steiner, P. W. Fowler, *Org. Biomol. Chem.*, **2006**, *4*, 2473.

[18] E. Steiner, P. W. Fowler, *Org. Biomol. Chem.*, **2004**, *2*, 34.

[19] a) M. Mandado, *Theor. Chem. Acc.*, **2010**, *126*, 339. b) S. Fias, S. Van Damme, P. Bultinck, *J. Comput. Chem.*, **2008**, *29*, 358. c) S. Fias, S. Van Damme, P. Bultinck, *J. Comput. Chem.*, **2010**, *31*, 2286. d) S. Fias, P. W. Fowler, J. L. Delgado, U. Hahn, P. Bultinck, *Chem.Eur. J.*, **2008**, *14*, 3093. e) R. Ponec, S. Fias, S. Van Damme, P. Bultinck, I. Gutman, S. Stanković, *Collec. Czech. Chem. Comm.*, **2009**, *74*, 147.

[20] *Calculation of NMR and EPR parameters: Theory and Applications*, (Eds: M. Kaupp, M. Buhl and V.G. Malkin), Wiley-VCH, Weinheim, Germany, **2004**.

[21] a) T. A. Keith, R. F. W. Bader, *Chem. Phys. Lett.*, **1993**, *210*, 223. b) T. A. Keith, R. F. W. Bader, *J. Chem. Phys.*, **1993**, *99*, 3669.c) S. Coriani, P. Lazzeretti, M. Malagoli, R. Zanasi, *Theor. Chim. Acta*, **1994**, *89*, 181. d) E. Steiner, P. W. Fowler, *Int. J. Quant. Chem.*, **1996**, *60*, 609.

[22] a) E. Steiner, P. W. Fowler, *J. Phys. Chem. A*, **2001**, *105*, 9553. b) E. Steiner, P. W. Fowler, R. W. A. Havenith, *J. Phys. Chem. A*, **2002**, *106*, 7048.

[23] a) P. W. Fowler, M. Lillington, L. P. Olson, *Pure Appl. Chem.*, **2007**, *79*, 969. b) E. Steiner, P. W. Fowler, *Phys. Chem. Chem. Phys.*, **2004**, *6*, 261.

[24] a) S. Bosanac, I. Gutman, *Z. Naturforsch.*, **1977**, *32a*, 10. b) I. Gutman, S. Bosanac, *Tetrahedron*, **1977**, *33*, 1809.

[25] I. Gutman, *Monatsh. Chem.*, **2005**, *136*, 1055.

[26] a) A. T. Balaban, J. Đurđević, I. Gutman, S. Jeremić, S. Radenković, *J. Phys. Chem. A*, **2010**, *114*, 5870. b) S. Radenković, J. Đurđević, I. Gutman, *Chem. Phys. Lett.*, **2009**, *475*, 289. c) I. Gutman, S. Stanković, J. Đurđević, B. Furtula, *J. Chem. Inf. Mod.*, **2007**, *47*, 776.

[27] a) J. Aihara, *J. Am. Chem. Soc.*, **1976**, *98*, 2750. b) I. Gutman, M. Milun, N. Trinajstic, *J. Am. Chem. Soc*., **1977**, *99*, 1692.

[28] a) J. Aihara, *J. Am. Chem. Soc.*, **1995**, *117*, 4130. b) J. Aihara, *J. Chem. Soc. Perkin Trans. 2*, **1996**, 2185.

[29] a) J. Aihara, *J. Phys. Chem.*, **1995**, *99*, 12739. b) J. Aihara, T. Ishida, H. Kanno, *Bull. Chem. Soc. Jap.*, **2007**, *80***,** 1518. c) J. Aihara, *J. Phys. Chem. A*, **2008**, *112*, 4382.

[30] F. A. Van-Catledge, *J. Org. Chem.*, **1980**, *45*, 4801.

[31] a) P. Bultinck, R. Ponec, S. Van Damme, *J. Phys. Org. Chem.*, **2005**, *18*, 706. b) M. Mandado, M. J. González-Moa, R. A. Mosquera, *J. Comput. Chem.*, **2007**, *28*, 127.

[32] a) R. S. Mulliken, *J. Chem. Phys.* **1955**, *23*, 1833. b) R. S. Mulliken, *J. Chem. Phys.* **1955**, *23*, 1841. c) R. S. Mulliken, *J. Chem. Phys.* **1955**, *23*, 2338. d) R. S. Mulliken, *J. Chem. Phys.* **1955**, *23*, 2343.

[33] a) M. Giambiagi, M. S. de Giambiagi, C. D. dos Santos, A. P. de Figueiredo, *Phys. Chem. Chem. Phys.*, **2002**, *2*, 3381. b) C. G. Bollini, M. Giambiagi, M. S. de Giambiagi, A. P. Figueiredo, *J. Math. Chem.*, **2000**, *28*, 71.

[34] P. Bultinck, R. Ponec, A. Gallegos, S. Fias, S. Van Damme, R. Carbó-Dorca, *Croat. Chem. Acta*, **2006**, *79*, 363.

[35] J.-I. Aihara, *J. Am. Chem. Soc.*, **2006**, *128*, 2873.

[36] a) P. v. R. Schleyer, C. Maerker, A. Dransfeld, H. Jiao, N. J. R. Eikema Hommes, *J. Am. Chem. Soc.*, **1996**, *118*, 6317. b) P. v. R. Schleyer, M. Manoharan, Z. Wang, X. B. Kiran, H. Jiao, R. Puchta, N. J. R. Eikema Hommes, *Org. Lett.*, **2001**, *3*, 2465.

[37] Gaussian 03, Revision C.02, M. J. Frisch, G. W. Trucks, H. B. Schlegel, G. E. Scuseria, M. A. Robb, J. R. Cheeseman, J. A. Montgomery, Jr., T. Vreven, K. N. Kudin, J. C. Burant, J. M. Millam, S. S. Iyengar, J. Tomasi, V. Barone, B. Mennucci, M. Cossi, G. Scalmani, N. Rega, G. A. Petersson, H. Nakatsuji, M. Hada, M. Ehara, K. Toyota, R. Fukuda, J. Hasegawa, M. Ishida, T. Nakajima, Y. Honda, O. Kitao, H. Nakai, M. Klene, X. Li, J. E. Knox, H. P. Hratchian, J. B. Cross, V. Bakken, C. Adamo, J. Jaramillo, R. Gomperts, R. E. Stratmann, O. Yazyev, A. J. Austin, R. Cammi, C. Pomelli, J. W. Ochterski, P. Y. Ayala, K. Morokuma, G. A. Voth, P. Salvador, J. J. Dannenberg, V. G. Zakrzewski, S. Dapprich, A. D. Daniels, M. C. Strain, O. Farkas, D. K. Malick, A. D. Rabuck, K. Raghavachari, J. B. Foresman, J. V. Ortiz, Q. Cui, A. G. Baboul, S. Clifford, J. Cioslowski, B. B. Stefanov, G. Liu, A. Liashenko, P. Piskorz, I. Komaromi, R. L. Martin, D. J. Fox, T. Keith, M. A. Al-Laham, C. Y. Peng, A. Nanayakkara, M. Challacombe, P. M. W. Gill, B. Johnson, W. Chen, M. W. Wong, C. Gonzalez, and J. A. Pople, Gaussian, Inc., Wallingford CT, 2004.

[38] C. Van Alsenoy, A. Peeters, *J. Mol. Struct. (Theochem)*, **1993**, *286*, 19.

[39] a) P. W. Fowler, E. Steiner, *Chem. Phys. Lett.*, **2002**, *364*, 259. b) G. Monaco, R. G. Viglione, R. Zanasi, P. W. Fowler, *J. Phys. Chem. A*, **2006**, *110*, 7447.

[40] a) P. Bultinck, M. Mandado, R. A. Mosquera, *J. Math. Chem.*, **2008**, *43*, 111. b) M. Mandado, R. A. Mosquera, *Chem. Phys. Lett.*, **2009**, *470*, 140.

[41] a) M. Randić, *Chem. Phys. Lett.* **1976**, *38*, 3839. b) J. A. N. F. Gomes, R. B. Mallion, *Rev. Port. Quim.* **1979**, *21*, 82. c) M. Randić, *Chem. Rev.* **2003**, *103*, 3449.

[42] M. Mandado, M. J. González-Moa, R. A. Mosquera, *J. Comput. Chem.*, **2007**, *28*, 1625.

[43] M. Mandado, *J. Chem. Theory Comput.*, **2009**, *5*, 2694.

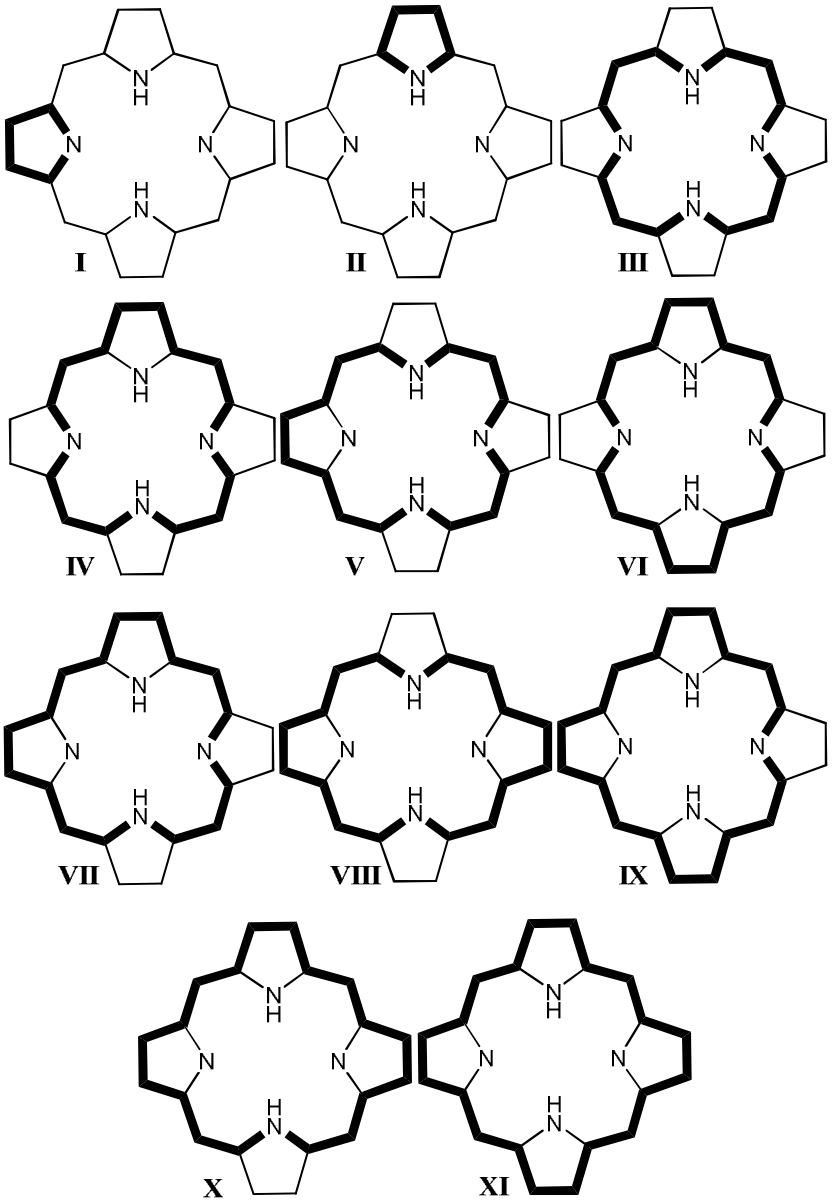

Figure 1. Ring circuits in porphin

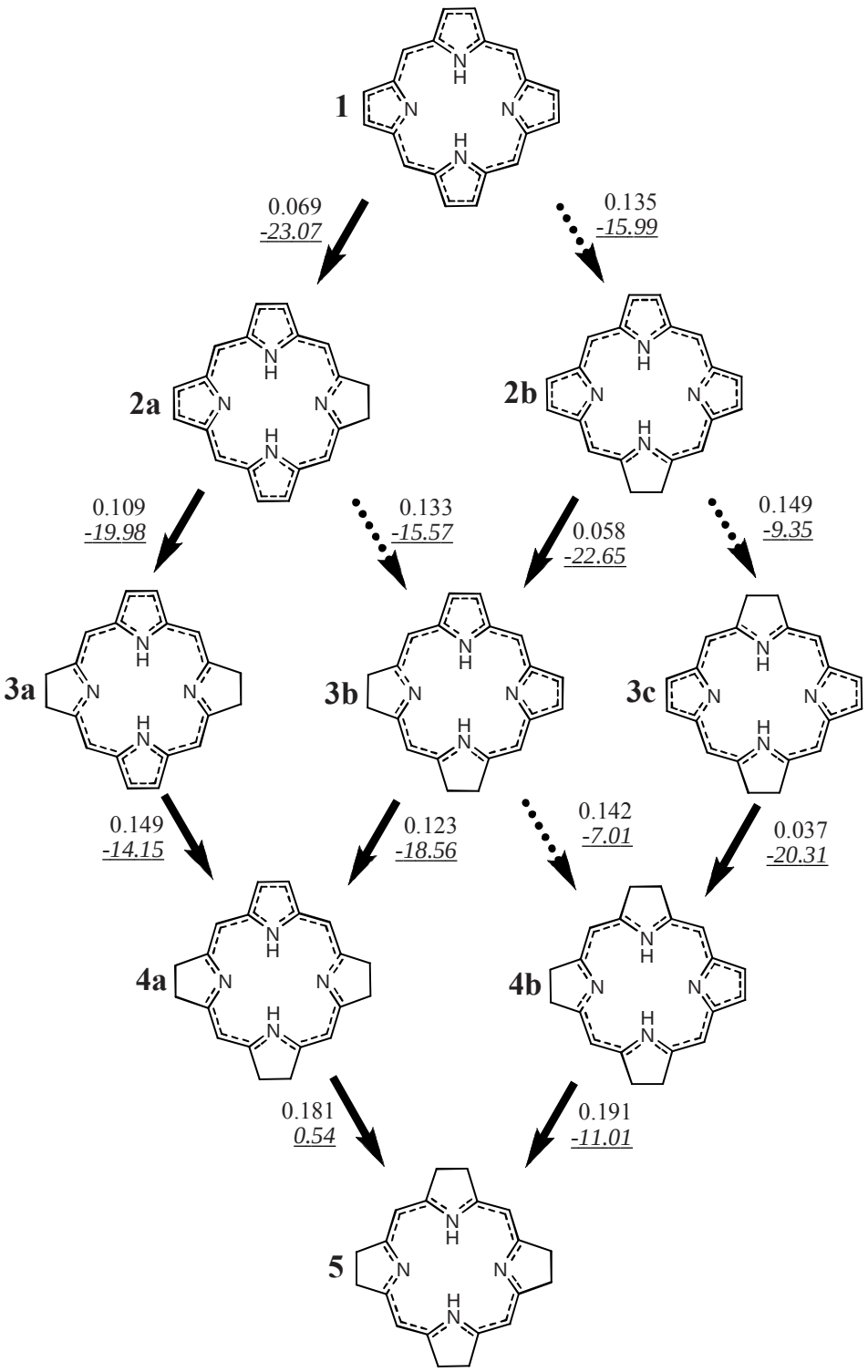

Figure 2. Hydrogenation paths linking porphin (**1**) with octahydroporphin (**5**), *BREs* for the C-C bonds involved in the hydrogenation (in β units, see text) and B3LYP/6-31++G(d,p) hydrogenation energies (underlined, in kcal·mol^{-1}). Solid arrow indicates the thermodynamically favoured path whereas the unfavoured one is indicated with a dashed arrow

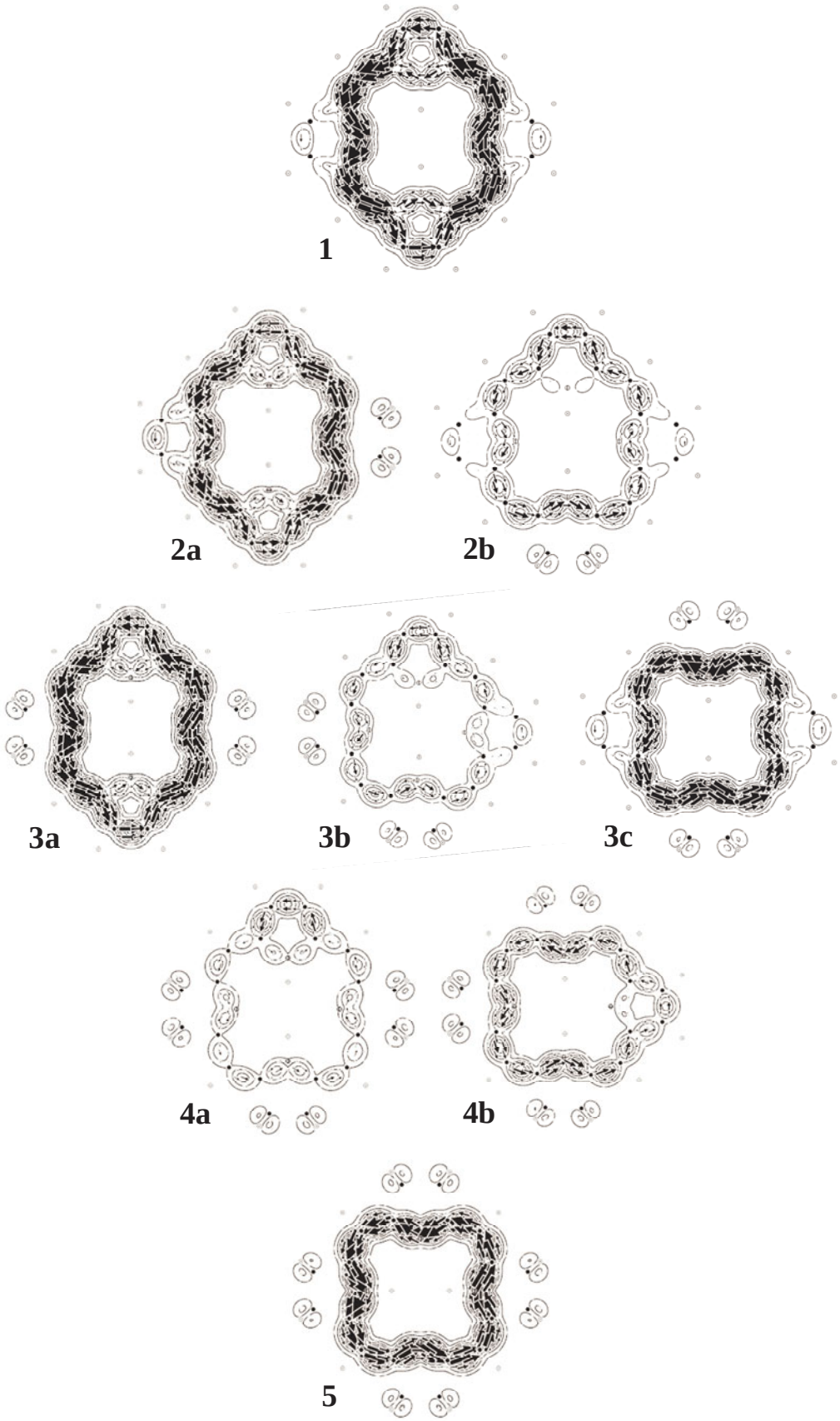

Figure 3. FO-CPHF/STO-3G π ring current plots obtained at 1Å above the molecule

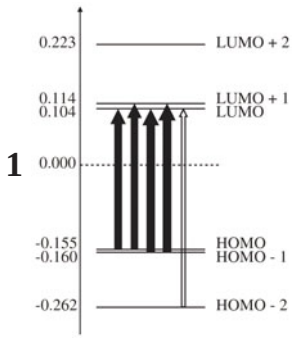
1
0.223
LUMO + 2
0.114
0.104
LUMO + 1
LUMO
0.000
-0.155
-0.160
HOMO
HOMO - 1
-0.262
HOMO - 2

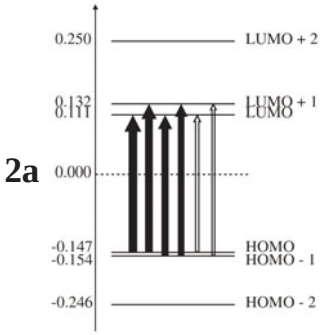
2a
0.250
LUMO + 2
0.132
0.111
LUMO + 1
LUMO
0.000
-0.147
-0.154
HOMO
HOMO - 1
-0.246
HOMO - 2

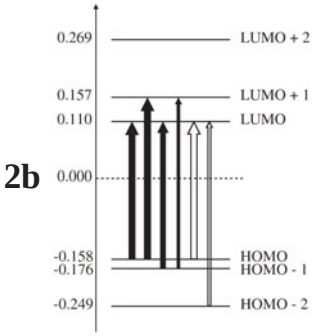
2b
0.269
LUMO + 2
0.157
0.110
LUMO + 1
LUMO
0.000
-0.158
-0.176
HOMO
HOMO - 1
-0.249
HOMO - 2

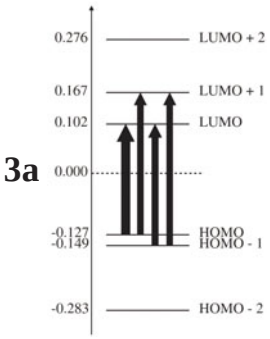
3a
0.276
LUMO + 2
0.167
0.102
LUMO + 1
LUMO
0.000
-0.127
-0.149
HOMO
HOMO - 1
-0.283
HOMO - 2

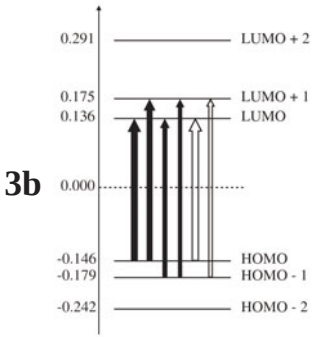
3b
0.291
LUMO + 2
0.175
0.136
LUMO + 1
LUMO
0.000
-0.146
-0.179
HOMO
HOMO - 1
-0.242
HOMO - 2

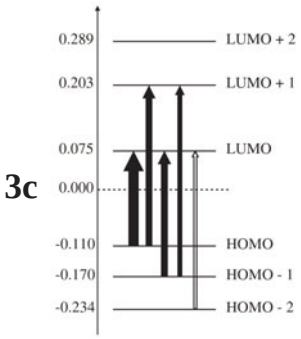
3c
0.289
LUMO + 2
0.203
LUMO + 1
0.075
LUMO
0.000
-0.110
HOMO
-0.170
HOMO - 1
-0.234
HOMO - 2

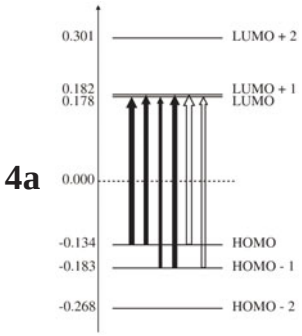
4a
0.301
LUMO + 2
0.182
0.178
LUMO + 1
LUMO
0.000
-0.134
HOMO
-0.183
HOMO - 1
-0.268
HOMO - 2

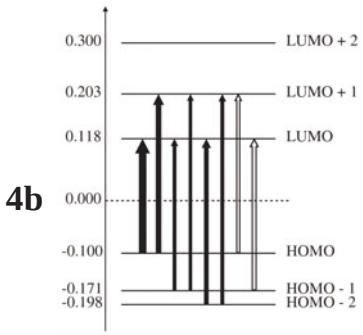
4b
0.300
LUMO + 2
0.203
LUMO + 1
0.118
LUMO
0.000
-0.100
HOMO
-0.171
HOMO - 1
-0.198
HOMO - 2

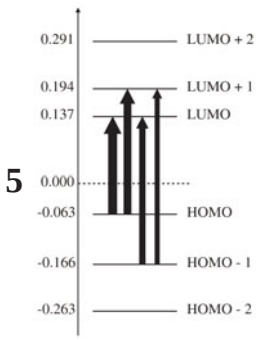
5
0.291
LUMO + 2
0.194
LUMO + 1
0.137
LUMO
0.000
-0.063
HOMO
-0.166
HOMO - 1
-0.263
HOMO - 2

Figure 4. Translational (diatropic, black arrows) and rotational (paratropic, arrows without filling) transitions between individual pairs of an occupied and virtual orbital for all molecules. Only significant contributions based on expressions (2) and (3) are shown and the width of the arrow reflects the magnitude of the contribution to the total current. The vertical axis denotes orbital energies (in au)

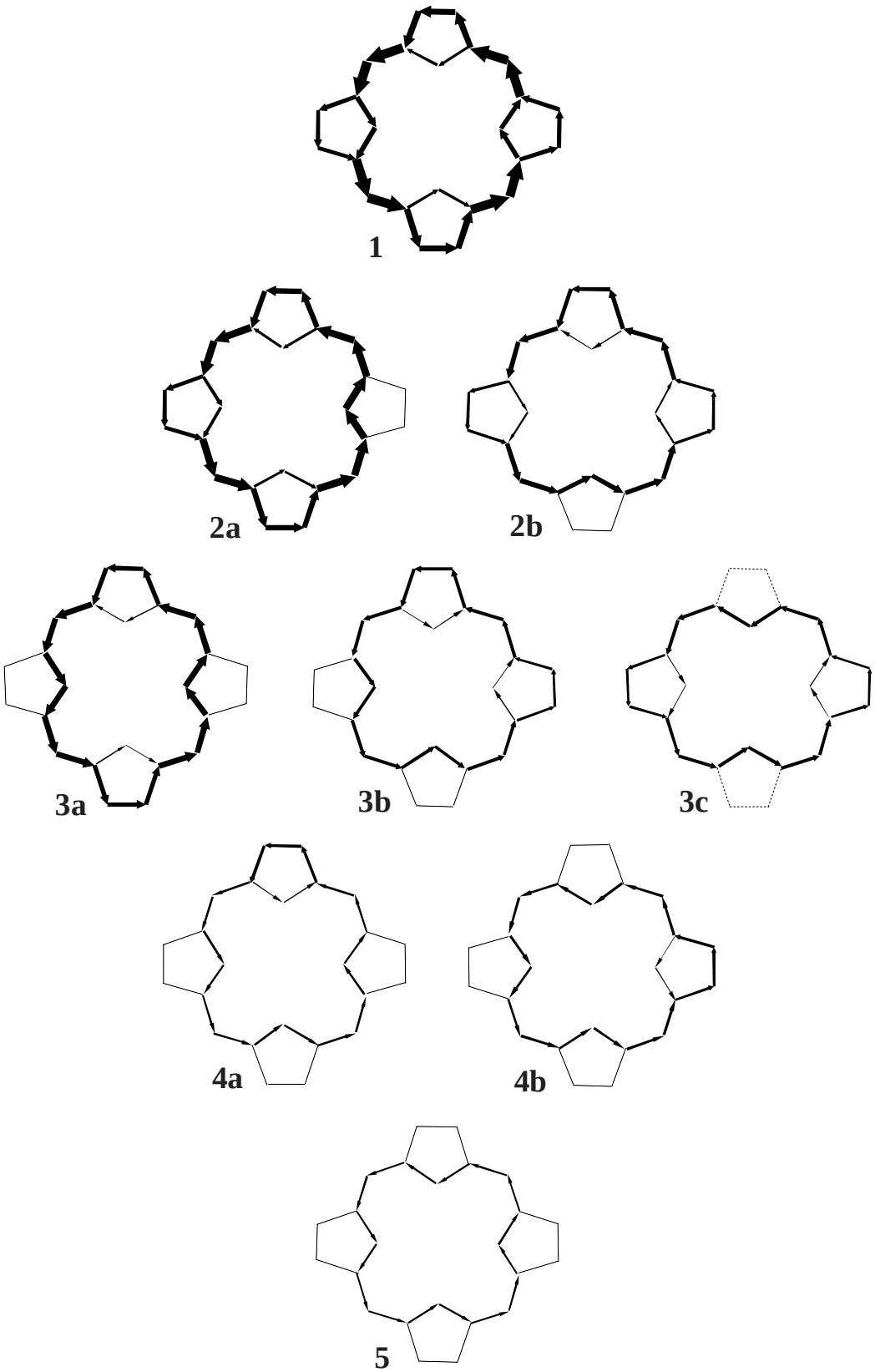

Figure 5. Pictorial representation of the ring currents obtained from multicenter indices

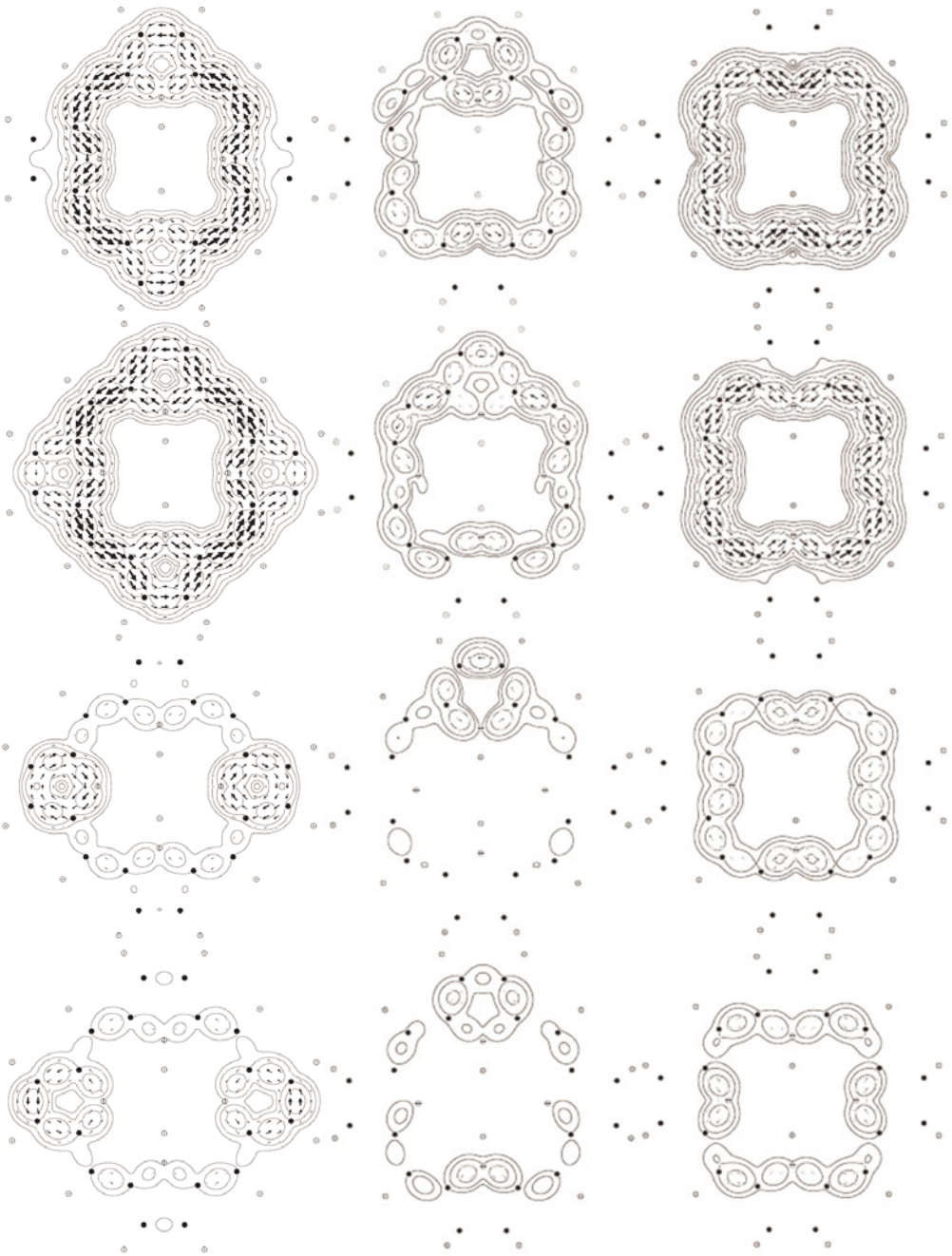

Figure 6. Orbital resolved ring currents for molecules **1**, **4a** and **5** (from left to right). In the figure are represented the contributions from the HOMO, HOMO-1, HOMO-2 and HOMO-3 (from up to down)

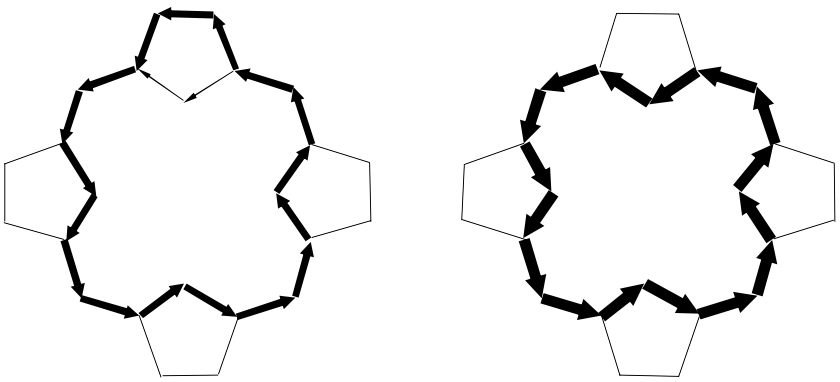

Figure 7. Pictorial representation of the ring currents obtained from *ef*(*Z*) values for molecules **4a** (left) and **5** (right)

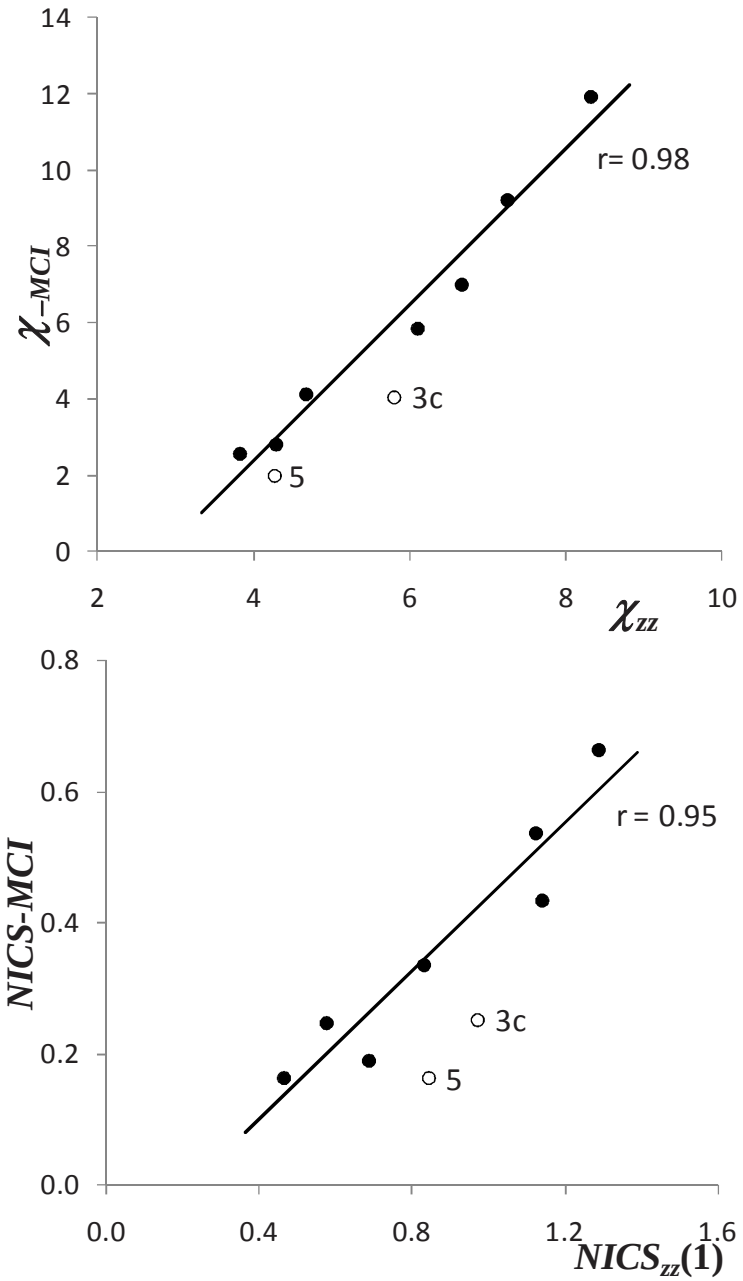

Figure 8. Correlation between the magnetic susceptibility exaltation estimated from multicenter indices and the *zz* component of the magnetic susceptibility tensor calculated at the B3LYP/6-31++G(d,p) level (upper plot), and correlation between the *NICS* estimated from multicenter indices and the $NICS_{zz}(1)$ calculated at the B3LYP/6-31++G(d,p) level at the center of ring circuits of type III in Figure 1 (lower plot). All values are given relative to the corresponding value for isolated benzene

Table 1. B3LYP/6-31++G(d,p) molecular electronic energies, *E*, topological resonance energies, *TRE*, and molecular symmetries. *E* is given in au and *TRE* in β units (see text).

Mol	Symmetry	*E*	*TRE*
1	D_{2h}	-989.61198	0.4322
2a	C_{2v}	-990.82771	0.3955
2b	C_2	-990.81659	---
	C_{2v}[a]	-990.81643	0.3319
3a	D_{2h}	-992.03853	0.3172
3b	C_1	-992.03173	---
	C_s[a]	-992.03150	0.3087
3c	C_{2h}	-992.01061	---
	D_{2h}[a]	-992.01031	0.2280
4a	C_2	-993.24051	---
	C_{2v}[a]	-993.24006	0.2407
4b	C_2	-993.22223	---
	C_{2v}[a]	-993.22165	0.2140
5	C_{2h}	-994.41895	---
	D_{2h}[a]	-994.41816	0.0770

[a] Structures with the C-N skeleton in planar conformation

Table 2. *ef*(*Z*) and *CRE-MCI* values calculated for the ring circuits depicted in Figure 1. All values are given in β units (see text). Values for circuits with no π-conjugation are not included because of being zero or close to zero (in the case of *CRE-MCI*).

Mol/Ring		I	II	III	IV	V	VI	VII	VIII	IX	X	XI
1	*ef*(*Z*)	0.0450	0.0799	0.0075	0.0100	0.0034	0.0130	0.0042	0.0013	0.0052	0.0015	0.0017
	CRE-MCI	0.0713	0.0764	0.0062	0.0069	0.0029	0.0076	0.0032	0.0014	0.0036	0.0015	0.0017
2a	*ef*(*Z*)	0.0808	0.0806	0.0064	0.0086	0.0033	0.0114	0.0041	---	0.0051	---	---
	CRE-MCI	0.0796	0.0767	0.0069	0.0080	0.0036	0.0093	0.0048	---	0.0042	---	---
2b	*ef*(*Z*)	0.0392	0.1016	0.0102	0.0134	0.0047	---	0.0059	0.0019	---	0.0023	---
	CRE-MCI	0.0718	0.0966	0.0063	0.0078	0.0031	---	0.0038	0.0015	---	0.0019	---
3a	*ef*(*Z*)	---	0.0894	0.0099	0.0138	---	0.0188	---	---	---	---	---
	CRE-MCI	---	0.0812	0.0081	0.0099	---	0.0122	---	---	---	---	---
3b	*ef*(*Z*)	0.1013	0.1022	0.0116	0.0162	0.0063	---	0.0081	---	---	---	---
	CRE-MCI	0.0815	0.0995	0.0066	0.0085	0.0036	---	0.0048	---	---	---	---
3c	*ef*(*Z*)	0.0196	---	0.0292	---	0.0129	---	---	0.0052	---	---	---
	CRE-MCI	0.0858	---	0.0104	---	0.0055	---	---	0.0029	---	---	---
4a	*ef*(*Z*)	---	0.1319	0.0187	0.0276	---	---	---	---	---	---	---
	CRE-MCI	---	0.1110	0.0065	0.0094	---	---	---	---	---	---	---
4b	*ef*(*Z*)	0.1532	---	0.0204	---	0.0067	---	---	---	---	---	---
	CRE-MCI	0.1082	---	0.0111	---	0.0072	---	---	---	---	---	---
5	*ef*(*Z*)	---	---	0.0770	---	---	---	---	---	---	---	---
	CRE-MCI	---	---	0.0156	---	---	---	---	---	---	---	---

Table 3. *zz* component of the magnetic susceptibility tensor, χ_{zz}, and $NICS_{zz}(1)$ values calculated at the B3LYP/6-31++G(d,p) level. Values for the hydrogenated pyrrol rings are not included because of being non-aromatic rings. Values of χ_{zz} are given relative to the value of isolated benzene, $NICS_{zz}(1)$ values are in ppm.

Mol	χ_{zz}	$NICS_{zz}(1)$[a]	$NICS_{zz}(1)$[b]	$NICS_{zz}(1)$[c]
1	8.33	-37.4	-32.2	-12.9
2a	7.26	-32.6	-32.1	-16.8
2b	6.10	-24.1	-30.6	-14.7
3a	6.68	-33.0	-35.3	---
3b	4.67	-16.7	-29.3	-18.2
3c	5.81	-28.2	---	-19.1
4a	3.83	-13.5	-31.1	---
4b	4.29	-19.9	---	-25.2
5	4.27	-24.5	---	---

[a] Calculated at the center of ring circuits of type III (see Figure 1)
[b] Calculated at the center of ring circuits of type II (see Figure 1)
[c] Calculated at the center of ring circuits of type I (see Figure 1)